Earth System
Science
Data
Open Access
Discussions

Snapshots of ice-free season dynamics in the near-shore water column of the northern Gulf of St. Lawrence, Canada

Emilie Arseneault[1,2], Neha Joshi[2,3], Julie Carrière[4], Émilie Saulnier-Talbot[1,2,3]

[1]Biology Department, Université Laval, Québec, QC, G1V 0A6, Canada
[2]Québec-Océan and Institute of Integrative Biology and Systems, Université Laval, Québec, QC, G1V 0A6, Canada
[3]Geography Department, Université Laval, Québec, QC, G1V 0A6, Canada
[4]Northern Institute for Research in Environment and Occupational Health and Safety (INREST), Sept-Îles, QC, G4R 2B2, Canada

Correspondence to: Emilie Arseneault (emilie.arseneault.3@ulaval.ca)

Abstract. Coastal ecosystems are highly dynamic and vulnerable to both climate changes and anthropogenic pressures. The Sept-Îles region, located in the northwestern Gulf of St. Lawrence, is a high-use subarctic coastal system with diverse urban, industrial and maritime activities. This study presents analyses of monthly water column profiles at 35 sites focusing on temperature, salinity and chlorophyll fluorescence, used as a proxy of phytoplankton biomass, during the ice-free season. Using a conductivity, temperature and depth (CTD) sensor, water column profiles were collected from May to October 2022 along the coastline, at sites between 2- and 52- meters depth. Results revealed a thermocline developing in spring, intensifying in summer and disappearing in autumn. Chlorophyll *a* (Chl *a*) concentrations peaked below the thermocline in July, while secondary increases were recorded at the surface in September, consistent with observations of an autumn bloom in similar environments. These findings highlight the complex dynamic of physical and biological parameters in the coastal water column, and the importance of the timing of sampling to fully capture seasonal variability. To improve future research in the area, measuring nutrient concentrations would be essential for detecting potential upwelling events and better explaining phytoplankton variation during summer. This study provides a valuable baseline for future investigations and justifies the continuation of measurements of water column variability in the region, in the context of rapid climate change. The complete dataset is available via https://doi.org/10.5683/SP3/ALRWON (Arseneault & Saulnier-Talbot, 2025a).

1 Introduction

Coastal environments are at the forefront of climate change impacts, experiencing diverse types of alterations due to rising global temperatures and anthropogenic activities (IPCC, 2023). These changes are noticeable in the Gulf of St. Lawrence, where sea ice cover has declined markedly over the past decade (Galbraith et al., 2024a). This trend, linked to rising winter air temperatures over the past few decades, highlights the region's sensitivity to global warming, which is expected to lead to increasingly ice-free conditions in the near future (Galbraith et al., 2024a). The Sept-Îles region, located in the northwestern Gulf of St. Lawrence, represents an economically vital area, hosting the most important mineral port in North America (PSI,

2025). Because of its industrial importance, the area is susceptible to several anthropogenic drivers (Beauchesne et al., 2020), in addition to rapid climatic changes. Among these, the disappearance of seasonal sea-ice is the most evident(Allard et al., 2025). In an effort to better understand the changing dynamics of the coastal ecosystem, several biodiversity studies are being conducted in the region's aquatic environment, covering diverse topics such as benthic communities (Dreujou et al., 2020; Joshi et al. 2025), intertidal and coastal diatoms (Arseneault et al., 2023; Arseneault & Saulnier-Talbot, 2025b), algal and bacterial pigments (Lefebvre, 2023; Araújo et al., 2022), microbial sedDNA (Bélanger, 2024), and sea-ice ecology (Allard et al., 2025). Regular environmental monitoring has also been undertaken (Carrière et al., 2018a; Ferrario et al., 2022), and the Bay of Sept-Îles (BSI) is currently part of the Enviro-Actions program, allowing a near real-time monitoring of industrial port zones (Carrière and Dreujou, 2024). In this context, understanding the hydrological characteristics of the Sept-Îles region (Shaw et al. 2022) and the dynamics of the water column is crucial for tracking the variability, rate, direction and intensity of environmental change over time.

Among the most significant features of the water column, the thermocline, a water layer at which temperature decreases rapidly with depth, plays a key role in regulating stratification. This division of the water column into different layers can create barriers for organisms (Fiedler, 2010). Seasonal stratification regulates phytoplankton dynamics, with spring blooms commonly observed in temperate waters, including the BSI (Roden and Raine, 1994; Araújo et al., 2022; Lim et al., 2025). Most studies focusing on water column layers are usually carried out in deeper areas, far from the coast (de Boyer Montégut et al., 2004; Galbraith, 2006). However, evidence of stratified water columns in shallow coastal areas has also been documented. For example, on the west coast of Ireland, stratification within 10 km of the shore was observed (Roden and Raine, 1994) and in southern waters of Korea, thermal stratification was found to occur at sites between 5- and 30-m depths (Lim et al., 2025). Despite these findings, studies on shallow-water stratification remain scarce.

Given the combination of climatic and direct anthropogenic pressures in this region, understanding the physical and biological baseline conditions of the aquatic environment is essential for assessing potential ecological transformations that could affect the food web and impact ecosystem services, such as fisheries and tourism. This study aimed to characterize the water column profiles in the Sept-Îles region by analyzing spatial and temporal variations in key oceanographic parameters during the ice-free season. By linking these observations to broader environmental drivers, the results will serve as a baseline for understanding ongoing changes and support studies aimed at monitoring and mitigating the effects of the various pressures in this coastal zone. The dataset generated in this study also represents a valuable resource for future research and management initiatives as it can be reused for projects related to coastal monitoring. Additionally, it contributes to initiatives such as the "Chaire de recherche sur les écosystèmes côtiers et les activités portuaires, industrielles et maritimes" (or EcoZone Chair, at Université Laval), which seeks to improve knowledge on coastal ecosystem functioning and to ensure sustainable management of these ecosystems subjected to port, industrial and maritime activities.

Water column profiles were collected once per month between May and October 2022, with a conductivity, temperature and depth (CTD) sensor. We emphasized the description of temperature, salinity and fluorescence. The latter was used as an indicator of phytoplankton biomass based on chlorophyll a (Chl a) concentrations recorded by the instrument. These profiles

70   provided valuable insights into the stratification and mixing dynamics that shape the physical environment of the region. The main objectives of this study are to describe the water column profiles, and to analyze their spatial and temporal dynamics. We also aim to investigate thermocline patterns and Chl a distribution to gain a better understanding of how temperature and primary production co-vary in this region throughout the ice-free season.

75   **2 Material and methods**

2.1 Study area

The study area covers the coastline of the Sept-Îles region, between 66°56' N and 65°54' W (Fig. 1). Situated in the
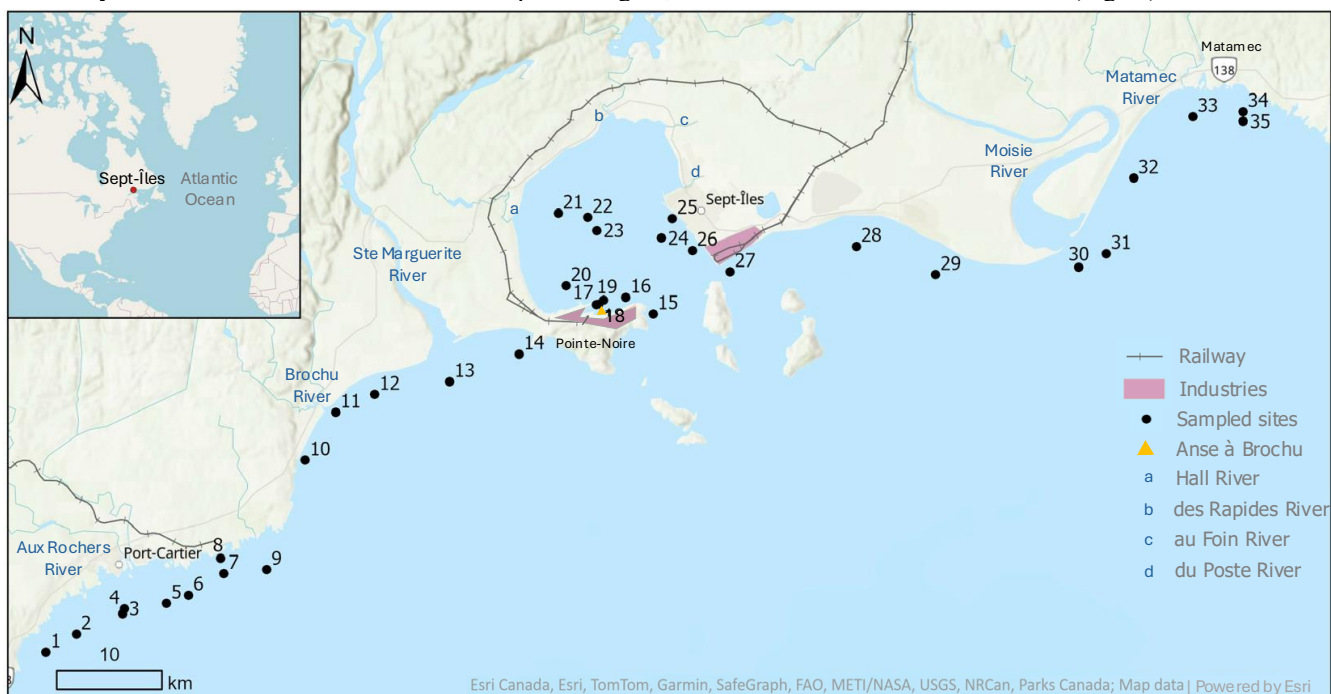

80   **Figure 1: Map of the location of the 35 sites sampled around Sept-Îles and major rivers of the region.**

northwestern Gulf of St. Lawrence, this region features a mix of saltwater brought by the Atlantic Ocean and freshwater from the St. Lawrence River and its tributaries (Lapointe, 2000; Carrière et al., 2018b). The region is under a semi-diurnal tidal system where tides range between 0.39 m to 3.6 m in Port-Cartier and 0.43 to 3.36 m in Sept-Îles (Fisheries and Ocean Canada,

85   2024). The area has a subarctic climate and has historically been covered by sea ice between November and April (Aubut

Demers et al., 2018). However, this period has been shrinking rapidly, and nearly ice-free winters could become more common due to climate warming (Galbraith et al., 2024a). Since 2010, the Gulf of St. Lawrence has experienced 4 winters with nearly ice-free conditions around the end of the season (Galbraith et al., 2024a).

90   According to a study on the hydrodynamics of the BSI (Shaw et al., 2022), the area exhibits an estuarian circulation pattern. Currents are seaward at the surface (2-10 meters) and shoreward in deeper waters (10-30 meters). Surface drifter measurements indicate average and maximum speeds of 17.4 cm s^{-1} and 86.6 cm s^{-1}, respectively. While locally dominated by tides, currents in the bay result from complex interactions between tides, estuarine circulation, winds, and the Earth's rotation. Water residence time is estimated to be 5.6 ± 3.5 days.

95

Diverse types of land-use along the transect were observed: natural coastlines with less developed areas, residential areas (urban and suburban) and Industrial-Port (IP) Zones. Sites 5 to 8 in Port-Cartier are located in an IP zone, and the Port of Sept-Îles is the second largest Canadian port for annual activity (PSI, 2025) where several heavy industries contribute to the economic importance of the region. The Matamec sector presents a less developed and more pristine environment, featuring

100 an ecological reserve and the Matamec River, which is of great conservation value (Government of Quebec, 2011). The study area is affected by freshwater input from the Ste-Marguerite and Moisie rivers, damned and wild, respectively. Smaller rivers also flow in the area, including the rivière aux Rochers in Port-Cartier and Brochu River, West of the Ste-Marguerite. The Hall, des Rapides, aux Foins and du Poste rivers flow into the BSI, with around 22 m^3 s^{-1} of freshwater input into this area annually (Shaw et al., 2019).

105 **2.2 Water sampling**

Water column profiles of temperature, salinity, turbidity, fluorescence, and photosynthetically active radiation (PAR) were directly measured using a Sea-Bird Electronics Conductivity-Temperature-Depth (CTD) instrument with two added Seapoint sensors, one for turbidity and one for fluorometry (i.e., Chl a). Chl a is an indicator of phytoplankton biomass and reflects the level of primary production in coastal waters (Araújo et al., 2022). The CTD was equipped with an integrated software system

110 that automatically calculated practical salinity, density, specific volume anomaly, Brunt-Vaisala frequency, Sigma-T, potential temperature, Sigma-Theta, freezing temperature, sound velocity, and absolute salinity. At each site, the CTD was lowered to approximately 2-3 m above the seafloor to prevent potential damage to the instrument. Measurements along the transect were made monthly at all sites between May and October 2022, (24th to 26th of May, 14th to 15th of June, 19th to 21st of July, 16th to 17th of August, 13th to 14th of September and 24th of October), except at site 34 in May and site 25 in June due to technical

115 problems. The dataset is available at https://doi.org/10.5683/SP3/ALRWON (Arseneault & Saulnier-Talbot, 2025a). Meteorological data for the week prior to sampling was also documented (Table 1). To facilitate visualizations, the 35 sites were divided into three Zones (Table 1). Sites 1 to 15 between Port-Cartier and the west of the BSI were defined as Zone 1, sites inside the BSI (16 to 27) were defined as Zone 2, and Zone 3 encompasses the sites from the east of the BSI to Matamec

(28 to 35). Monthly vertical profiles of temperature, salinity, turbidity and fluorescence at each site were generated using 120 "ggplot" (R core Team, 2022). With the same statistical package, relationships between Chl a and

Table 1: Site zones and description of land use.

Site number	Zone	Land use	Mean depth of profile (m)
1	1	Forest	11.5
2	1	Forest	12.2
3	1	Urban	13.2
4	1	Urban	11.7
5	1	IP zone	15.3
6	1	IP zone	16
7	1	IP zone	16.3
8	1	IP zone	10.2
9	1	Forest/IP zone	25.5
10	1	Residential	8
11	1	Brochu River	5.7
12	1	Beach-Residential	19.3
13	1	Ste-Marguerite River	21.3
14	1	Beach/Forest	19.2
15	1	Beach/Forest	19.8
16	2	IP zone	19.8
17	2	IP zone/Anse à Brochu	3.3
18	2	IP zone/Anse à Brochu	7.8
19	2	IP zone/Anse à Brochu	20.2
20	2	IP zone	14.8
21	2	Ship mooring zone	13
22	2	Ship mooring zone	14.2
23	2	Ship mooring zone	16.7
24	2	Urban	9.8
25	2	Urban	3
26	2	Urban-IP zone	23.2
27	2	IP zone	30.5
28	3	Beach/Forest	15
29	3	Beach/Forest	14.3
30	3	Moisie River	28.7

31	3	Moisie River	48.3
32	3	Beach/Forest	16.2
33	3	Matamec River	15.2
34	3	Ecological reserve	15
35	3	Ecological reserve	24.8

environmental variables were explored. Scatter plots with LOESS curves to observe general trends were generated and
125   Spearman correlation was used to assess the significance of these relationships.

## 2.2 Determination of the thermocline

Thermocline layers were identified, if possible, monthly at every site. Determining the depths of the thermocline is not always
straightforward, as several methods can be used (de Boyer Montégut et al., 2004). These methods are however rarely applied
in areas as shallow as in this study. Janecki et al. (2022) found no studies of this sort except in the Baltic Sea, where depths
130   still reached 100 m (Leppäranta and Myrberg, 2009). These authors developed a new algorithm for shallow seas to find the
top of the thermocline and halocline, for sites reaching >100 m. We decided for this study to use the gradient threshold method
of 0.2 °C (de Boyer Montégut et al., 2004; Leppäranta and Myrberg, 2009). We assumed that the top layer of the thermocline
was located at the depth of the strongest gradient of the slope ($\Delta T > 0.2$ °C), and the lower layer was located at the depth of
the deepest gradient, to capture the typical plateau, if there was one. Since the sites in our study area were shallow, between 4
135   and 52 m with an 18 m median, we decided to start the calculations at 3 m depth instead of the advised near-surface 10 m
depth (de Boyer Montégut et al., 2004). This approach also avoided the possible effects of the instrument, the anchor and the
boat, which can mix the surface waters (de Boyer Montégut et al., 2004; Maske et al., 2014). The depths of the thermocline
layer were obtained with the package "rLakeAnalyzer" (Winslow et al., 2019), with some modifications of the "therm.depth"
function. A cutoff of 1 °C was also applied, a default criterion in the R function. If the change between surface and maximum
140   depth temperatures was less than this threshold, thermocline depth was not calculated. Thermocline depths were not calculated
for sites with a maximum depth < 5 m. The results were verified visually to confirm the method used and to assess if
temperature changes aligned with the salinity changes. We chose to use temperature to define the layers since some
measurements of salinity were not recorded by the CTD. Lim et al. (2025), also focused on thermocline while carrying out a
study on a similar environment with dynamic coastal waters influenced by water masses and anthropogenic activities. One site
145   out of the 35 was chosen to present the vertical profiles of temperature, salinity, Chl *a* and PAR in detail during the season.

3 Results

3.1 Temperature and thermocline

In May, temperature was the coldest and was mostly even across depth at all sites (Fig. 2). Surface temperature averaged 5.56
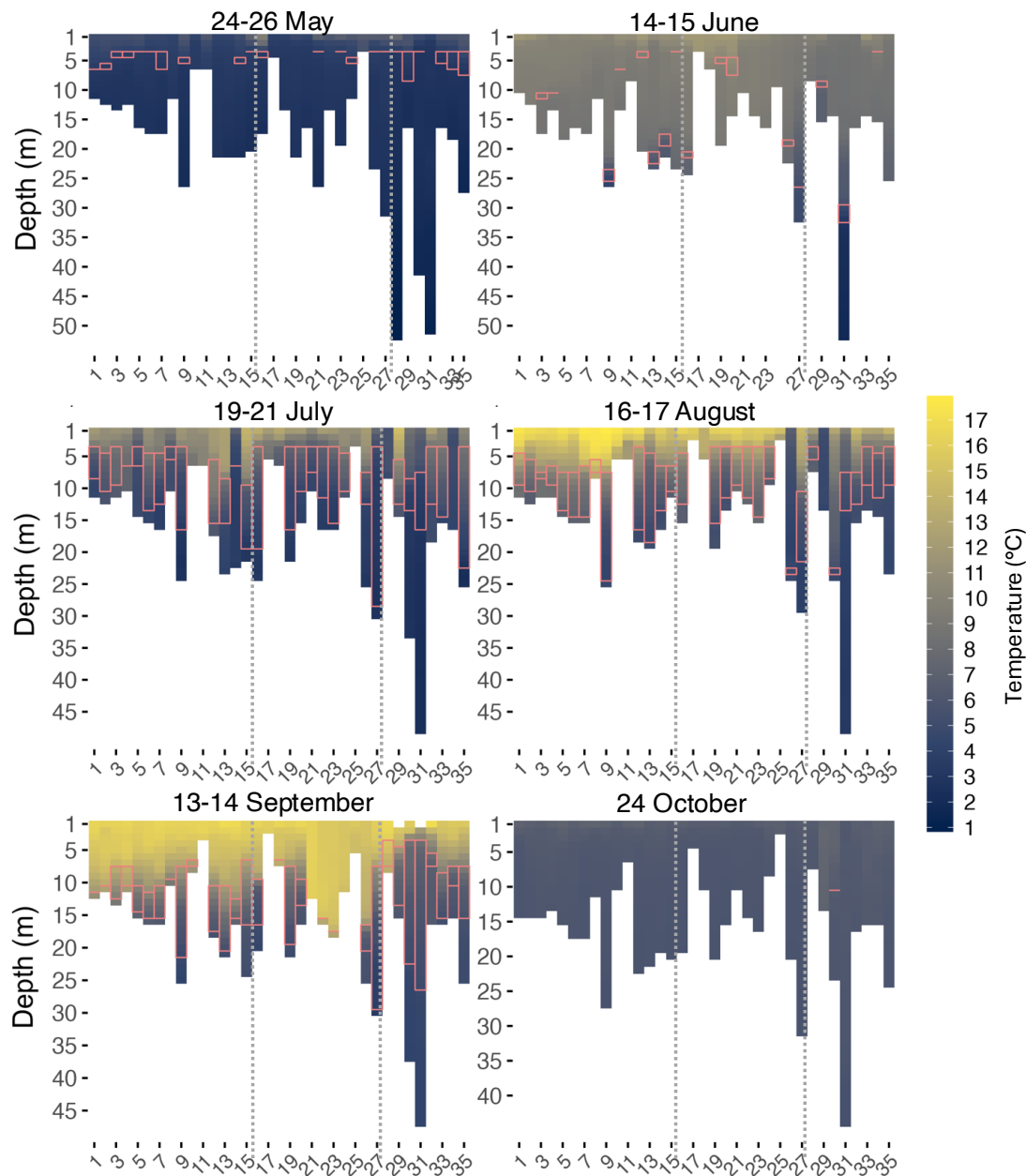
Figure 2: Temperature heatmaps for every month at every site (x axis) along the transect. Dotted lines indicate division of Zones 1
150 **(West), 2 (BSI), and 3 (East), from left to right. The pink rectangles represent the thickness of the thermocline layer.**

°C along the transect. At maximum depth, temperatures ranged between 0.85 °C (Site 31) and 3.83 °C (Site 11), excluding site 25 which was only 3 meters deep. During this period, a near-surface thermocline was beginning to form (Fig. 2 and 3), usually between 3- and 4- m depth. In May, 22 sites showed the onset of stratification. In June, surface temperatures began to

155 rise, ranging from 8.69 °C (site 32) to 11.99 °C (site 19). The water column remained largely mixed, but stratification
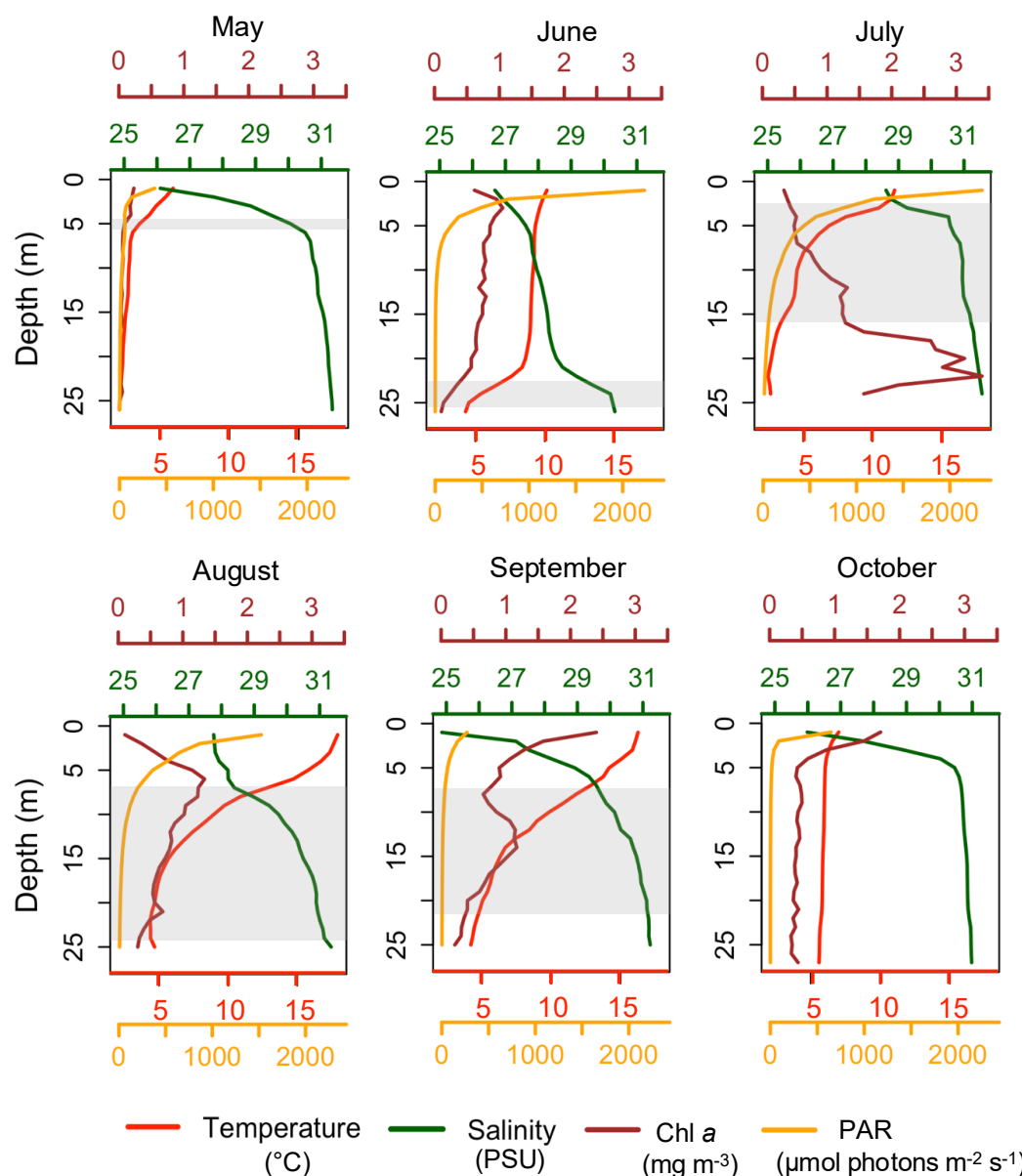

Figure 3: Vertical profiles of temperature, salinity, Chl *a* and PAR at Site 9, on each sampling date. The gray box represents the thermocline layer.

Earth System
Science
Data
Open Access Discussions

became noticeable at deeper sites, such as sites 9, 27 and 31, where temperatures were between 1.72 °C (Site 31) and 4.3 °C (Site 9) at maximum depth. Sixteen sites exhibited thin thermocline layers (1-2 m thick), mostly near the bottom of the water

160   column. Waters in June were generally well-mixed.

Between July and September, clear stratification developed with increasing temperatures, though a few shallow sites, < 6 meters depth, lacked distinct layers. At most sites in July, a thermocline was observed between 4 m and 5 m depth. Surface temperatures ranged from 5.52 °C (Site 28) to 14.80 °C (Site 29). While surface warming was observed at some sites, 14 sites

165   recorded a colder surface temperature than in June. For instance, recorded temperature at site 34 was 10.15 °C in June versus 5.63 °C in July. Temperature became colder at shallower depths in July, contrasting with June's well mixed conditions where colder waters only appeared at the deepest sites. In August, surface temperatures ranged between 5.18 °C (Site 29) and 17.92 °C (Site 9). Stratification was still persistent but started to deepen. August showed a deepening of the thermocline: up to 4 m at some sites (5 and 6) in the west, while sites in the BSI, like sites 19 to 24, showed the same depth layers as in June. At the

170   eastern sites, the thermocline deepened between 4 and 12 meters. September marked the warmest month throughout the water column, although deeper sites like sites 31, 30 and 9 retained colder bottom temperatures, around 4.2 °C. At several western sites, the thermoclines continued to deepen, while they began to disappear at the BSI sites and became shallower toward the east, near the Moisie River (sites 30 and 31). By October, the entire transect showed uniform temperatures with no significant differences between surface and maximum depths, and the absence of a thermocline. In early fall, the overall mean surface

175   temperature was 6.83 °C, with 5.55 °C at maximum depth, resulting in an average difference of only 1.28°C throughout the water column. All sites were mixed, except for site 31, the deepest one, that showed a weak persistent thermocline at around 10 meters depth.

In summary, surface temperatures increased from May to September, with stratification becoming prominent in July. By

180   October, conditions in the transect had reversed back to cold, uniform temperatures across depths. The largest changes in surface temperatures occurred between May and June (increase of 5.02 °C), and September and October (a decrease of 9.30 °C). Site 9 was chosen as an example (Fig. 3) to show how the thermocline layer, using the threshold method, matched with the vertical profiles of temperature and other parameters. This site was approximately 25 meters deep and did not have any NA (not available) values, making the visualization easier. At this specific site, the thermocline, as observed in general, started

185   to appear in May at a shallow depth, deepened during summer and disappeared in October.

3.2 Salinity

Signals of freshwater input at sites near river mouths were apparent in May (Fig. 4), particularly at sites 29 (17.8 PSU), 31 (19.7 PSU) and 30 (20.1 PSU), located near Moisie River. These sites recorded the lowest surface salinity, likely due to increased volume of river discharge following spring snowmelt. The overall average salinity of the water column in May was

190   30.0 PSU. June recorded an average of 27.8 PSU, the lowest salinity of the season. In contrast, July showed the highest with
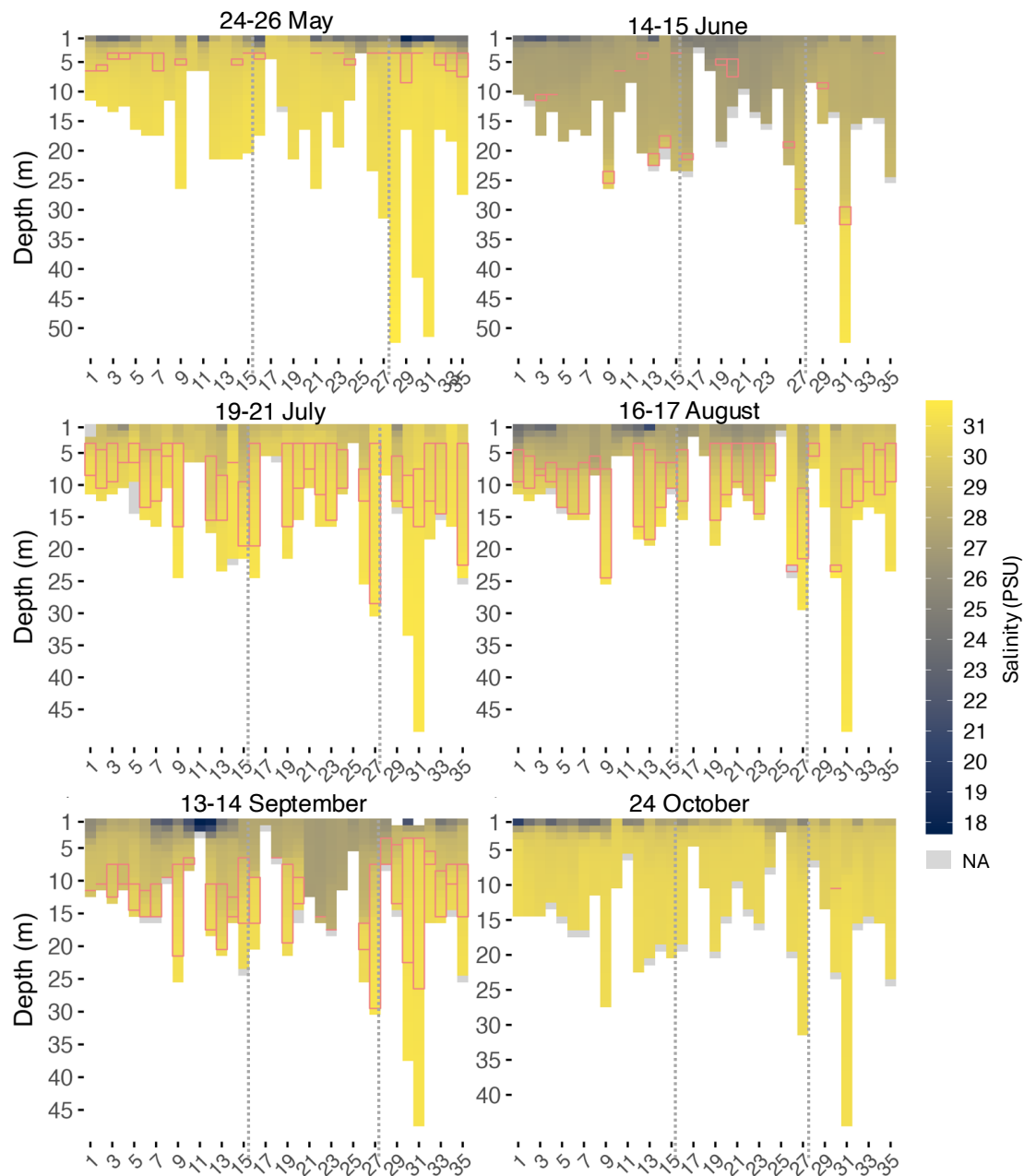
Figure 4: Salinity heatmaps for every month at every site (x axis) along the transect. Dotted lines indicate division of Zones 1 (West), 2 (BSI), and 3 (East), from left to right. The pink rectangles represent the thickness of the thermocline layer.

an average salinity across sites around 30.6 PSU. Stratification became more visible at some sites in July where salinity was lower above the thermocline, such as sites 13 and 15, that recorded 28 PSU versus 30 PSU below. In August, salinity above

195 the thermocline decreased to around 27 PSU, showing the deepening of stratification. A strong signal of freshwater input by rivers was again observed in September, this time near the Brochu and Ste-Marguerite Rivers, at sites 11 (17.6 PSU) and 12

(19.1 PSU). In October, salinity was more uniform below the surface, while surface salinity remained lower, especially at sites located west of the transect, where salinity at Site 1 reached 20 PSU at the surface. Below surface, salinity increased to over 30 PSU along the water column.

200

In these data, salinity inversely followed temperature trends in the water column, where it increased with depth while temperature decreased. This relationship was visible in vertical profiles such as Site 9 (Fig. 3). A Spearman correlation analysis confirmed that temperature and salinity were inversely correlated across the dataset (r = -0.84, p-value < 0.01). Overall, salinity at maximum depth showed little seasonal variation, averaging over 30 PSU, except in June (28.5 PSU). The most pronounced
205 seasonal differences in salinity were observed at surface. May and June had the lowest surface salinities whereas July had the highest salinity, and August only showed a slight decrease, in general. A drop in surface salinity was observed in September, especially at sites near the Brochu River (Site 11). Salinity exhibited variability at the surface (first 2 meters), usually at sites located near rivers, and became uniform at depth.

3.3 Turbidity

210 Because turbidity mostly varied at surface, only data down to a depth of 5 meters was shown for better clarity (Fig. 5). Turbidity across the transect varied between 0 and 8.4 FTU with limited variability, except at certain sites mostly located inside the BSI (sites 16 to 21). These sites showed a turbidity range of 4.8 to 8.4 FTU, with the highest value measured at site 20.

215 Higher values of turbidity, superior to 2 FTU, were also recorded in May, in the BSI and at sites near river mouths, such as sites 11 (4.6 FTU), 30 and 31. A similar pattern was observed in October, with higher turbidity values in the BSI and at sites close to rivers, where Site 20 exhibited a surface turbidity of 3.2 FTU and Site 11 a turbidity of 2.6 FTU. In July and September, turbidity remained below 2 FTU throughout the transect, with sites within the BSI being slightly more turbid than the others.
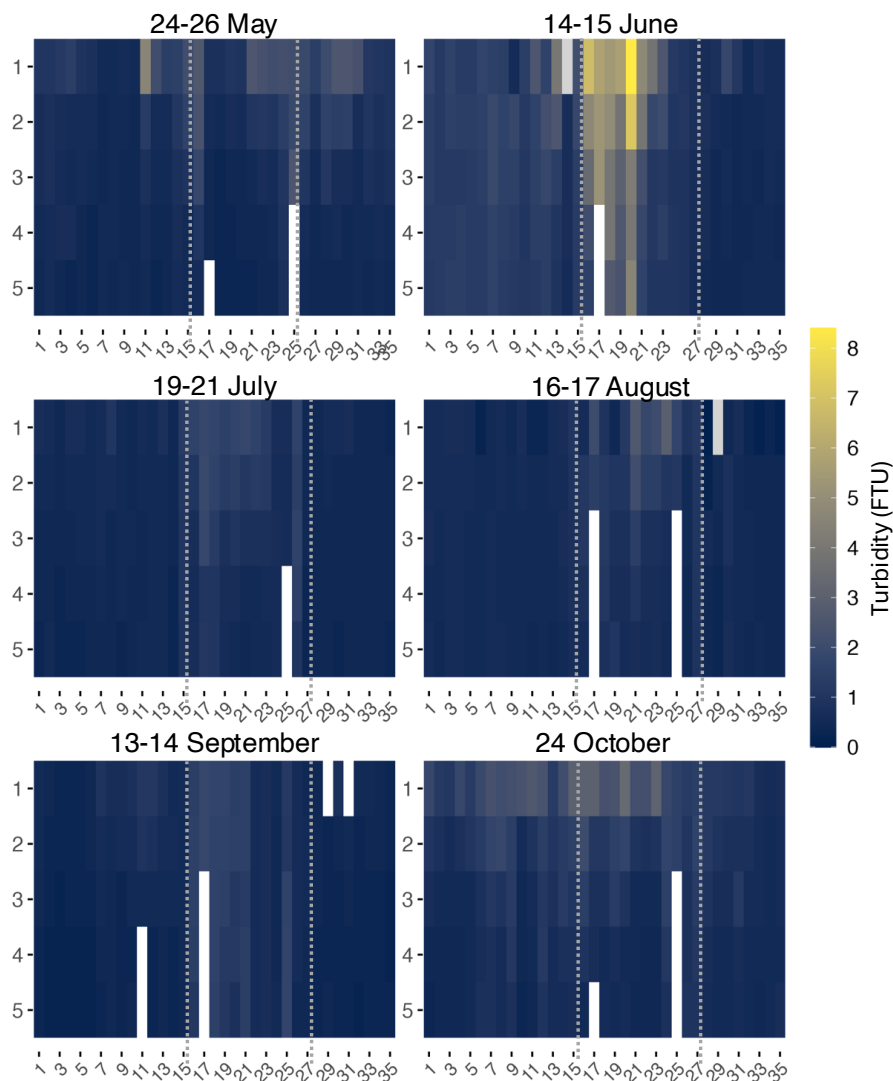
220

Figure 5: Turbidity heatmaps for every month at every site (x axis) along the transect. Dotted lines indicate division of zones 1 (West), 2 (BSI), and 3 (East), from left to right. The pink rectangles represent the thickness of the thermocline layer.

3.4 Fluorescence (Chl *a*) and PAR

A seasonal variation of fluorescence (Fig. 6), reflecting concentration of Chl *a*, was observed along the transect. Concentrations

225 were the lowest in May and began to rise in June, reaching a peak in July, and then decreased throughout August to October. In September, a localized resurgence was observed at the surface of some sites, before fluorescence levels declined again in October at most sites.
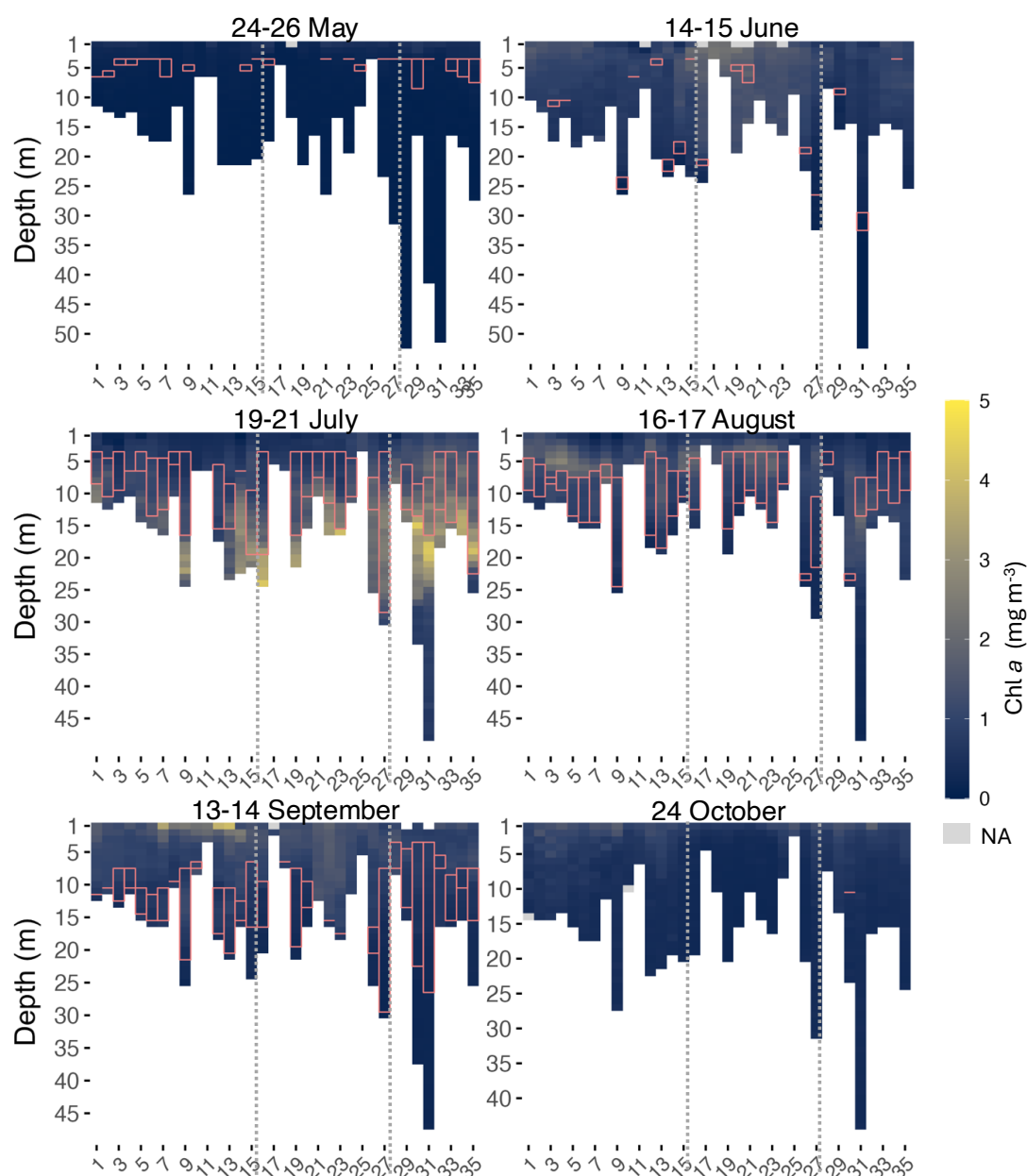
Figure 6: Chl *a* heatmaps for every month at every site (x axis) along the transect. Dotted lines indicate division of zones 1 (West), 2 (BSI), and 3 (East), from left to right. The pink rectangles represent the thickness of the thermocline layer.

230   In May, fluorescence throughout the transect averaged 0.097 mg m^{-3} and PAR 85.5 µmol photons m^{-2} s^{-1}. All sites had a concentration below 1 mg m^{-3} at all depths. In June, sites 17, 18 and 19 recorded the highest Chl *a* concentration. These were the only sites across the entire transect where fluorescence exceeded 2 mg m^{-3} in June, all between 1 and 3 meters. In July, the highest concentrations were found at sites 30, 31, 16, and 35, followed by Site 23 where concentrations were all superior to 4

mg m^{-3}, at depths between 15 to 24 meters. All these sites were located near rivers, except for Site 16 which was positioned in

235   front of an aluminum smelter. At this site, the highest concentration of 4.28 mg m^{-3} was measured at 24 meters, which was the

maximum depth at this site. All fluorescence peaks were below the thermocline layer, except at Site 35 where fluorescence

concentrations were higher at the thermocline. Average PAR in June (144 µmol photons m^{-2} s^{-1}) and July (145 µmol photons

m^{-2} s^{-1}) were similar but higher at the surface in June than in July (1,520 compared to 746 µmol photons m^{-2} s^{-1} in July).

August showed the highest PAR of the season, averaging 292 µmol photons m^{-2} s^{-1} overall, and 1,707 µmol photons m^{-2} s^{-1}

240   at surface, while fluorescence started to decline with an overall average of 0.94 mg m^{-3}. Sites 3, 4, 5, and 6, all located in Port-

Cartier near the aux Rochers River estuary, and Site 31 at the Moisie River, had a concentration superior to 2 mg m^{-3}. Maximum

fluorescence (2.73 mg m^{-3}) was observed at Site 4 at a depth of 5 m. Highest fluorescence in August occurred at shallower

depths than in July, between 5 and 26 m. In contrast to July, peaks of Chl a in August were mostly found at shallower depths,

either above or within the thermocline layer.

245

In September, sites 7 (3.49 mg m^{-3}), 12 (3.84 mg m^{-3}) and 13 (4.06 mg m^{-3}) recorded higher fluorescence concentrations than

in August, all at the surface. Concentrations higher than 2 mg m^{-3} were observed at 8 sites, all located in the western part of

the transect. Fluorescence declined again in October, with an average fluorescence of 1.11 mg m^{-3} overall. The maximum

fluorescence for this month (1.79 mg m^{-3}) was measured at the surface of Site 32, followed by the surface of Site 9 (1.71 mg

250   m^{-3}). October was also the month with the lowest mean PAR (35.7 µmol photons m^{-2} s^{-1}).

3.5 Relationship between Chl a and environmental variables (temperature, salinity, PAR and turbidity)

In this data set, temperature, salinity, turbidity and PAR all had significant effects on Chl a, and the scatterplots and LOESS

smoothers revealed nonlinear relationships (Fig. 7). The highest Chl a concentrations were mostly observed at colder

temperatures, particularly between 1 and 5 °C, and at higher salinities between 30 and 32 PSU. Concentrations then decreased

255   with increasing temperature, with a secondary rise at warmer values, as suggested by the trend. This could reflect the fewer

peaks of Chl a near the surface observed in autumn. A few additional peaks were detected at lower salinities (<24 PSU), likely

indicating the influence of localized riverine inflow and associated nutrients inputs. Peaks of fluorescence were most abundant

under low to moderate light conditions, between 0 and 100 µmol photons m^{-2} s^{-1}. When focusing on Chl a peaks only (>2 mg

m^{-3}), the relationship with PAR showed a weak negative correlation (r = -0.46, p<0.01) as opposed to a weak positive one with

260   all the data (r = 0.42, Fig.7). These peaks mostly occurred between 0.88 and 1,491 µmol photons m$^{-2 -1}$, with a median of 16.9

µmol photons m^{-2} s^{-1}. This was also visible at Site 9 (Fig. 3), where in July, peaks (>3 mg m^{-3}) were below the thermocline at

low PAR between 19.8 and 29.2 µmol photons m^{-2} s^{-1}. Turbidity measurements were mostly between 0 and 2 FTU during the

sampling period, which coincided with most of the Chl a peaks. Given the nonlinear nature of the relationships, Spearman

correlations only revealed moderate positive associations for all variables, except for salinity, which exhibited a negative trend.
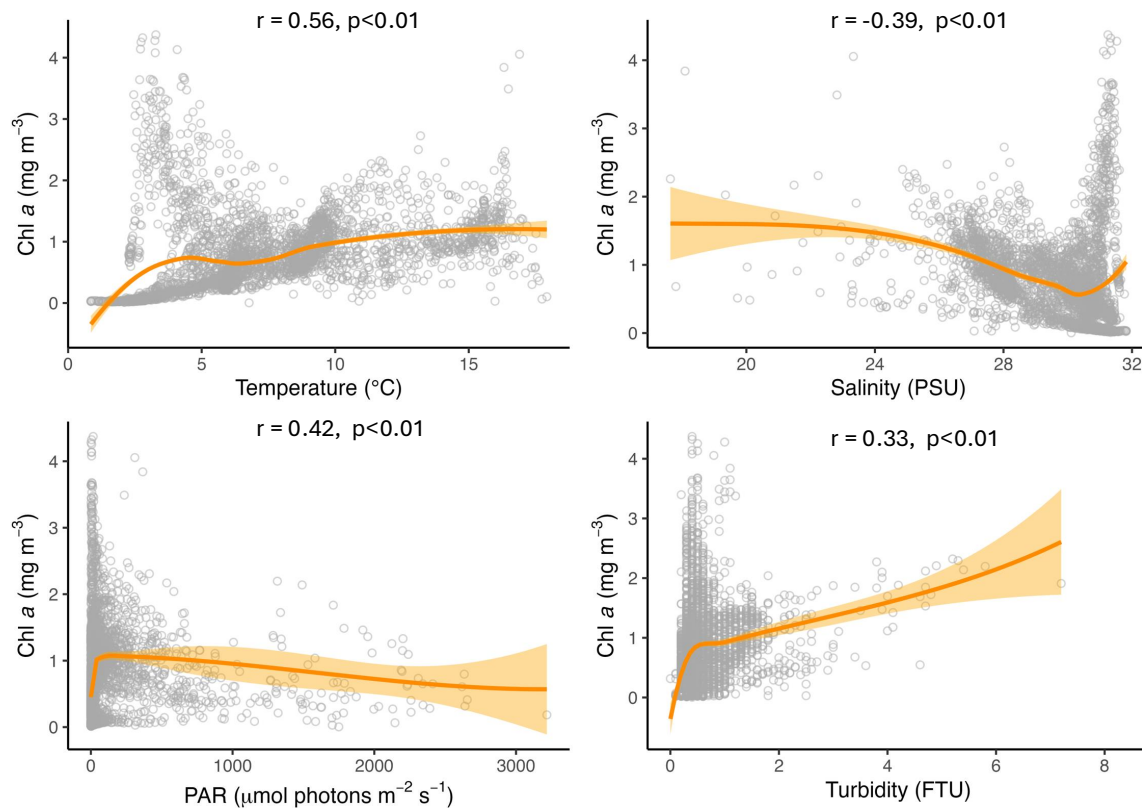
265

Figure 7: Scatter plots showing the relationships between Chl *a* and temperature, salinity, PAR and turbidity across the transect. The orange line represents the LOESS curve with 95% confidence interval (shaded area). The Spearman correlation (r) and its p-value are also indicated.

4 Discussion

This study shows that the water column properties near the coast of the Sept-Îles area undergo changes during the ice-free season, shifting from cold, well-mixed waters in spring to pronounced stratification in summer, particularly in July and August. The thermal stratification gradually deepens in September and disappears by October, with waters mixing and returning to more uniform conditions in autumn. Our study also highlights seasonal variability in Chl *a*, with high concentrations observed below the thermocline in July and fewer peaks observed at the surface in September near river sites. Most of the Chl *a* peaks recorded through the season, occurred at lower temperatures and higher salinity observed in July. Based on this dataset gathered in 2022, the Sept-Îles area shows typical seasonal variability of a temperate coastal environment (Cloern, 1991; Leppärante and Myrberg, 2009; Galbraith et al. 2024b; Lim et al., 2025). In the Gulf of St. Lawrence, phytoplankton blooms are generally observed in spring followed by a secondary bloom in autumn (Galbraith et al., 2024b). However, this pattern differs in the present study, since the main bloom was observed during summer, perhaps due to the fact that we did not sample at the end of

April, when the spring bloom might occur. Previous studies on pigments and phytoplankton assemblages carried out in the BSI, reported similar results; a seasonal variability in primary production with peaks of Chl *a* occurring in April, June and September (Lefebvre, 2023; Araújo et al., 2022). This seasonal dynamic may already be influenced by climate change. The Gulf of St. Lawrence, historically covered with sea-ice until mid-March, has experienced 4 nearly ice-free winters since 2010

285   (Galbraith et al., 2024a). Changes in sea-ice cover are also occurring in the BSI, where sea-ice has been disappearing sooner than usual over the past few years, and its formation and movements are becoming unpredictable (Allard, 2025). According to Allard (2024), these changes during the winter season could impact primary productivity in the BSI. Sea-ice changes can affect spring bloom timing and the composition of phytoplankton species, thus impacting the whole food web (Pärn et al., 2022; Castagno et al., 2023; Nielsen et al., 2024). A possible small trend towards an earlier and more intense spring bloom was

290   observed by Laliberté and Larouche (2023) between 1998 and 2019 in the St. Lawrence Estuary and Gulf, and they associated this trend with the decreasing length of the sea-ice season.

In May, temperature and salinity were stable across the water column, but a warmer and brackish surface layer started to develop, marking the beginning of thermocline formation. This layer is heated by the sun during summer, while freshwater

295   continues to flow from rivers into the area. As observed in our study, lower salinity was mostly found at localized places in proximity to rivers, e.g., sites 29, 30 and 31, near the Moisie River in May and sites 11 and 12 next to the Brochu and Ste-Marguerite rivers in September, all coinciding with peak river discharge (Carrière et al., 2018a). The influx of freshwater also increased turbidity at river-influenced sites such as Site 11, next to Brochu River. The well-mixed water column in May, and June, could also be linked to wind. Wind speeds recorded during these two months were stronger than those observed int the

300   other months (Table A1). Phytoplankton abundance remained minimal with fluorescence averaging 0.097 mg m^{-3}. Lefebvre (2023) identified April and May as the most productive months in the BSI during summer 2017, an observation that does not align with our study, as all concentrations of fluorescence were below 1 mg m^{-3} in May 2022. According to Araújo et al., (2022) the spring bloom in the BSI in 2017 occurred in April to early May before the spring freshet, where diatoms were the main phytoplankton group. Our first sampling was conducted at the end of May, between the 24th and the 26th, probably after

305   the spring bloom. Furthermore, Araújo et al. (2022) and Lefebvre (2023) using the same dataset, carried out their sampling mostly at the surface, whereas we measured the whole water column, which could be another reason explaining the differences in our results.

In mid-June, the water column was generally warmer, except at deeper sites such as Site 31, which reached 52 m in depth. A

310   deeper thermocline layer marked the limit between the warmer mixed layer and the colder, saltier deep waters. As for variation in Chl *a*, only a few sites (17, 18 and 19, all located in the BSI in front of Anse à Brochu) recorded a Chl *a* concentration exceeding 2 mg m^{-3}. These sites also recorded the highest turbidity and still showed highest concentrations of Chl *a* along the transect. Usually, turbidity limits phytoplankton biomass by reducing light penetration (Cloern, 1987; May et al., 2003). However, given the shallow depth at these sites, particularly sites 17 (2 m) and 18 (6 m), it is possible that the sampling process,

315 including boat anchoring and the use of the CTD instrument, contributed to sediment resuspension. It could have brought particles from the bottom layer to the surface and affected turbidity measurements. Wind, tides and waves can also have an influence at these shallow sites. Furthermore, the presence of phytoplankton or other organisms also affect turbidity measurements. However, such high turbidity levels were only observed in June. Another explanation could be the location of Anse à Brochu that is at proximity of industrial activities and private docks. This area is also next to a discharge point for

320 stormwater and municipal sewage discharge (Carrière et al., 2018b). Given the importance of these industries and the traffic of vessels, it is possible that these aspects contributed to sediment resuspension, influencing Chl a concentration. This also aligns with Lefebvre (2023), who observed a peak of Chl a (> 5 mg   m^{-3}) at this same location in June 2017, associated with a dinoflagellate bloom. Furthermore, Liu et al. (2018), found that in high turbidity environments, temperature had a greater impact than light intensity on the timing of blooms. This could potentially be the case in our study.

325

Thermal stratification appears to play an important role in structuring plankton communities. Lim et al. (2025) found that plankton diversity and richness in coastal waters of southern Korea were lowest in July, coinciding with strong thermocline formation, whereas diversity peaked in September when stratification weakened. Additionally, their results indicated that plankton abundances below the thermocline were significantly lower than in the upper layer. In contrast, our study found that

330 the highest Chl a concentrations were in July and were predominantly located below the thermocline. As seen in figures 2 and 7, the highest concentration of Chl a was deeper in the water column and at low to moderate PAR, but where nutrients are sufficient for growth. However, nutrients were not measured in the present study. In oceanic environments, Chl a concentration varies dynamically and often shows maximum values in the subsurface of the layer rather than at the surface (Yasanuka et al., 2022). In the East China Sea, similar results were found, where the highest Chl a concentrations were recorded at the bottom

335 of the thermocline. This was associated with a change in nutrient concentrations, where phytoplankton had access to a greater supply of nutrients at depth (Wu et al., 2002). Given that nutrient availability is a key driver for phytoplankton in the water column (Browning and Moore, 2023; Wei and Zhao, 2025), the higher Chl a concentrations below the thermocline in our study could potentially be explained by nutrient accumulation in deeper layers rather than light availability. However, some studies still find high Chl a concentrations even when nutrients are depleted, as observed in the Baltic Sea (Stramska and Jakacki,

340 2024). This suggests that other processes, such as upwelling events and currents, may also influence Chl a distribution. For example, at some locations of our transect, environmental conditions changed in July compared to June. Site 34, for example, recorded a decline in temperature from 10.2 °C to 5.63 °C during this time. Likewise, Site 31 (near the Moisie River) exhibited higher salinity in July than in June. Furthermore, most peaks of Chl a occurred at lower temperatures and high salinity (Fig. 7), suggesting potential upwelling events. Several areas in the Gulf of St. Lawrence, including the north shore of the Gulf, are

345 known to be in upwelling areas (Bourque and Kelley, 1995; Doyon and Ingram, 2000). These events are often associated with high Chl a concentrations, as they bring cold, nutrient-rich deep waters to the surface (Roegner et al., 2011; Diez-Minguito and de Swart, 2020). A 22-year time series by Laliberté and Lerouche (2023) showed a strong positive trend in Chl a along the Gulf's North Shore, that they associated with stronger upwelling events generated by favorable winds. Modeling studies

17

suggested that increased wind speeds may enhance upwellings along the north coast of the Gulf, potentially offsetting surface

350   warming (Long et al., 2016). Although no long-term data currently exists for our specific study area, the elevated wind speeds observed in July may have facilitated vertical mixing and nutrient transport, contributing to the observed Chl *a* maxima.

By August, we observed that the highest Chl *a* concentrations (>2 mg m^{-3}) had shifted above the thermocline. This shift may have been driven by surface heating, with observed temperatures increasing during summer between July and September. This

355   deepens the thermocline over time and alters vertical distribution patterns, contributing to variability in phytoplankton abundance. The surface layer in August also showed a lower salinity above the thermocline, reflecting river runoff and the beginning of the secondary summer bloom observed here and in earlier studies (Carrière et al., 2018a; Lefebvre, 2023).

September brought the warmest water temperatures of the year, likely due to heat accumulation over the summer months. Air

360   temperature reached its peak between mid-July and mid-August (Table A1), contributing to the deepening of the thermocline during this period. Despite differences between our spring results and those of Araújo et al. (2022) and Lefebvre (2023) in the BSI, we found similar results for September. Fluorescence showed surface peaks at sites 7, 12 and 13, located outside the BSI. Although these peaks were at different locations than those sampled by Lefebvre (2023), who focused on sites within the BSI, they still demonstrate that there is observable phytoplankton activity in early autumn. The location of these peaks also suggests

365   environmental influences. Site 7 is in proximity to the industrial zone of Port-Cartier, close to the outflow of several streams, and sites 12 and 13 are located near the Brochu River. The latter is of ecological significance as a highly productive salt marsh ecosystem is found at its mouth (Bourque and Malouin, 2009). These sites also exhibited freshwater influence since they represented the area along the transect with the lowest surface salinity, especially in September. However, turbidity at these sites remained relatively low, averaging only 1 FTU. This could indicate a peak in river discharge influencing phytoplankton

370   dynamics through nutrient inputs, that were not measured for this study. A study in a similar environment, a Chinese bay under anthropogenic effects, found that nutrients via river inputs had the greatest influence on Chl *a* concentrations (Wang et al., 2024).

Finally, the water column returned to well-mixed conditions in October, with fluorescence declining, and the complete

375   disappearance of the thermocline, with the exception of Site 30 that still showed a residual deep thermocline. In the first meter at surface along the transect, freshwater influence was still noticeable but did not impact the rest of the water column. October recorded higher turbidity at certain sites, mostly located within the BSI. The BSI has a counterclockwise circulation, which tends to concentrate freshwater discharges from the four rivers in the Pointe-Noire area (Shaw et al., 2022; Paquette et al., 2018). This circulation pattern likely explains the elevated turbidity in this area in October, while also accounting for the

380   absence of a freshwater signal despite the numerous streams and rivers flowing into the BSI.

5 Data availability

The complete CTD data used in this study are available in the Borealis database: https://doi.org/10.5683/SP3/ALRWON (Arseneault & Saulnier-Talbot, 2025a).

6 Conclusion

385 This study of water column dynamics during the ice-free season in a subarctic coastal environment documented seasonal variability of key ecological parameters including temperature, salinity and Chl *a*. The region of Sept-Îles has a highly dynamic coastal ecosystem where environmental conditions fluctuate daily. Although the typical spring bloom was not recorded, likely due to sampling starting after its peak, seasonal trends in thermocline formation and Chl *a* distribution were observed throughout the ice-free season. This clear seasonal variability has also been observed in similar environments such as the South

390 of the Baltic Sea, where a thermocline forms in the beginning of May and starts to deepen in September due to autumn cooling (Leppäranta & Myrberg, 2009). However, due to the dynamic nature of the study area and its shallow depths, thermoclines and observed water column trends can change within a day. For instance, Carrière et al. (2018a), could not detect a thermocline in the BSI in summer 2016, potentially due to sampling dates that may not have aligned with peak stratification periods. Furthermore, lowest salinity values occurred during spring and early fall, coinciding with peak river discharge. Paquette et al.

395 (2018) explained that these local freshwater layers can persist from a few hours to a few days in calm conditions. The results of our study depict the near-shore water columns at specific dates, as sampling was carried out only once per month. This shows how phytoplankton biomass variability is high in dynamic environments with complex physical parameters interactions, as previously suggested in similar studies (e.g. May et al., 2003).

400 Incorporating nutrient and oxygen monitoring would be essential to further improve our understanding of the mechanisms driving Chl *a* variability in the water column of this region and detecting potential upwelling events or eutrophication. Sept-Îles represents a high-use coastal ecosystem, under the influence of climatic and anthropogenic pressures, highlighting the importance of long-term and regular monitoring to detect environmental changes. Climate-related impacts such as changes in sea-ice cover, wind regimes and the intensity of upwelling events may influence primary productivity. Therefore, regular

405 monitoring of the water column, especially Chl *a*, is crucial to detect trends in phytoplankton dynamics and to assess broader ecological impacts of environmental change. This study complements prior work and will be useful for future studies and environmental monitoring in the region.

Appendices

410 **Table A1: Meteorological data for sampling days (in bold) and the previous week. Data retrieved from the Government of Canada at the Sept-Îles Station (Government of Canada, 2025). Temperatures are air temperature (no water temperature data is available).**

Dates	Max temp. (°C)	Min temp. (°C)	Mean temp. (°C)	Total precipitation (mm)	Max speed gust (km/h)
17/05/2022	5.9	4	4.9	31.7	58
18/05/2022	9.3	-1.8	3.8	2.9	53
19/05/2022	13.6	-2.5	5.6	0	<30
20/05/2022	14.1	3.7	8.9	0.3	<30
21/05/2022	8.7	7	7.9	6.1	31
22/05/2022	15.3	6	10.7	11.6	32
23/05/2022	13.7	-2.4	5.7	0	39
24/05/2022	**15.4**	**-2.8**	**6.3**	**0.3**	**<30**
25/05/2022	**19.3**	**0.6**	**9.9**	**0.6**	**39**
26/05/2022	**11.8**	**4.7**	**8.2**	**7.1**	**38**
07/06/2022	17	5.6	11.3	0	35
08/06/2022	14	9.3	11.6	14.3	54
09/06/2022	11.6	9.1	10.3	11	45
10/06/2022	12.3	9.2	10.8	18.2	44
11/06/2022	19.9	9.3	14.6	4	<30
12/06/2022	17.7	5.8	11.7	0	<30
13/06/2022	17.2	10.8	14	0.8	54
14/06/2022	**18.8**	**10.3**	**14.6**	**0.2**	**<30**
15/06/2022	**23.4**	**8.6**	**16**	**0**	**<30**
12/07/2022	17.5	13	15.3	25.7	<30
13/07/2022	22	6	14	0.2	42
14/07/2022	19.8	6.2	13	0	<30
15/07/2022	25.4	10.4	17.9	0	36
16/07/2022	19.5	10.9	15.2	0	<30
17/07/2022	22.6	10.4	16.5	0	<30
18/07/2022	21.5	13.9	17.7	0.5	<30
19/07/2022	**20.7**	**14.8**	**17.8**	**0**	**41**
20/07/2022	**26.3**	**14.5**	**20.4**	**0**	**46**
21/07/2022	**23.2**	**12.3**	**17.7**	**7.9**	**36**
09/08/2022	19.5	7.5	13.5	0.2	NA
10/08/2022	17.9	5.6	11.8	0.4	NA
11/08/2022	NA	NA	NA	NA	NA
12/08/2022	20.8	11	15.9	0.3	<30
13/08/2022	21.8	9.4	15.6	0.5	<30

14/08/2022	20.6	9.2	14.9	1.8	<30
15/08/2022	22.5	10	16.2	0.5	<30
16/08/2022	**25.6**	**11.3**	**18.4**	**0.2**	**<30**
17/08/2022	**24**	**14.1**	**19**	**0**	**<30**
06/09/2022	15.7	1.6	8.6	0	<26
07/09/2022	17.2	8.7	12.9	0	<30
08/09/2022	16.1	9.3	12.7	3.9	<30
09/09/2022	15.4	9.8	12.6	0.2	<30
10/09/2022	17.4	12.5	14.9	0	<30
11/09/2022	15.3	10.4	12.8	0	<30
12/09/2022	23	9.1	16	0.3	<30
13/09/2022	**17.4**	**11**	**14.2**	**0**	**<30**
14/09/2022	**16.5**	**11.4**	**13.9**	**12.5**	**45**
17/10/2022	12.6	2.6	7.6	0.3	<30
18/10/2022	9.4	6.7	8	20.5	63
19/10/2022	10.1	8.4	9.2	49.4	62
20/10/2022	9.1	4.1	6.6	3.6	<30
21/10/2022	8.6	4.7	6.7	0	34
22/10/2022	11.3	-0.3	5.5	0	<30
23/10/2022	16.4	-1.2	7.6	0	<30
24/10/2022	**11.7**	**0.5**	**6.1**	**0**	**<30**

Author contribution

EA and ÉST worked on the conceptualization and the methodology of this study. EA performed the formal analysis and visualization. EA and ÉST wrote the original draft and JC and NJ revised to the manuscript. ÉST and JC worked on the project

415 administration and funding acquisition.

Competing interests

The authors declare that they have no conflict of interest.

Acknowledgments

References

Allard, S.: Comprendre l'écosystème hivernal des zones portuaires subarctiques: le microbiome et les diatomées de la baie de Sept-Îles (Québec, Canada). M.S. thesis, Université Laval, Quebec, Canada, 2024.

430

Allard, S., Gosselin, M., and Saulnier-Talbot, É.: Winter diatom assemblage composition to track shrinking seasonal sea ice cover in a coastal subarctic bay (Quebec, Canada), Diatom Res., 1–20, https://doi.org/10.1080/0269249X.2025.2534359, 2025.

Arseneault, E., Pienitz, R., Carrière, J., and Saulnier-Talbot, É.: Insights into Diatom Substrate Preferences in the Inter-Tidal

435 Zone of a Subarctic Coast, Hydrobiology, 2, 537–553, https://doi.org/10.3390/hydrobiology2040036, 2023.

Arseneault, E., and Saulnier-Talbot, É.: Snapshots of ice-free season dynamics in the near-shore water column of the northern Gulf of St. Lawrence, Canada, Borealis, V1 [data set], https://doi.org/10.5683/SP3/ALRWON, 2025a.

440 Arseneault, E., and Saulnier-Talbot, É.: Species-environment relationships of coastal diatoms from the Sept-Îles region, Gulf of St. Lawrence (Québec, Canada), J. Phycol., https://doi.org/10.1111/jpy.70094, 2025b.

Araújo, C. A. S., Belzile, C., Tremblay, J.-É., and Bélanger, S.: Environmental niches and seasonal succession of phytoplankton assemblages in a subarctic coastal bay: Applications to remote sensing estimates, Front. Mar. Sci., 9, 1001098,

445 https://doi.org/10.3389/fmars.2022.1001098, 2022.

Aubut Demers, K., Le Hénaff, A. and Carrière, J.: État des glaces, in: Observatoire Environnemental de la Baie de Sept-Îles, edited by: Carrière, J., INREST, Sept-Îles, QC, Canada, 593–612, 2018.

450 Beauchesne, D., Daigle, R. M., Vissault, S., Gravel, D., Bastien, A., Bélanger, S., Bernatchez, P., Blais, M., Bourdages, H., Chion, C., Galbraith, P. S., Halpern, B. S., Lavoie, C., McKindsey, C. W., Mucci, A., Pineault, S., Starr, M., Ste-Marie, A.-S.,

and Archambault, P.: Characterizing Exposure to and Sharing Knowledge of Drivers of Environmental Change in the St. Lawrence System in Canada, Front. Mar. Sci., 7, https://doi.org/10.3389/fmars.2020.00383, 2020.

455 Bélanger, L.: Analyse spatiale et temporelle de la siversité microbienne dans la Baie de Sept-Îles, QC, M.S.thesis, Université Laval, Quebec, Canada, 2024.

Bourque, M. and Kelley, D. E.: Evidence of wind-driyen upwelling in jacques-cartier strait, Atmos.-Ocean, 33, 621–637, https://doi.org/10.1080/07055900.1995.9649548, 1995.

460

Bourque, M., and Malouin, J.: Guide d'intervention en matière de conservation et de mise en valeur des habitats littoraux de la MRC de Sept-Rivières, Comité ZIP Côte-Nord du Golfe, Canada, 155 pp., 2009.

Browning, T. J. and Moore, C. M.: Global analysis of ocean phytoplankton nutrient limitation reveals high prevalence of co-

465 limitation, Nat. Commun., 14, 5014, https://doi.org/10.1038/s41467-023-40774-0, 2023.

Carrière, J., and Dreujou, E: Projet Pilote Enviro-Actions, in : Actes du Symposium Enviro-Actions, edited by: INREST, 18, 2024.

470 Carrière, J., Le Hénaff, A., and Aubut Demers, K.A.: Qualité de l'eau, in: Observatoire Environnemental de la Baie de Sept-Îles, edited by: Carrière, J., INREST, Sept-Îles, QC, Canada, 83-211, 2018a.

Carrière, J., Le Hénaff, A., and Aubut Demers, K.: Description du site d'étude, in: Observatoire Environnemental de la Baie de Sept-Îles, edited by: Carrière, J., INREST, Sept-Îles, QC, Canada, 45-82, 2018b.

475

Castagno, A. P., Wagner, T. J. W., Cape, M. R., Lester, C. W., Bailey, E., Alves-de-Souza, C., York, R. A., and Fleming, A. H.: Increased sea ice melt as a driver of enhanced Arctic phytoplankton blooming, Global Change Biol., 29, 5087–5098, https://doi.org/10.1111/gcb.16815, 2023.

480 Cloern, J. E.: Turbidity as a control on phytoplankton biomass and productivity in estuaries. Cont. Shelf Res., 1367-1381, 1987.

Cloern, J. E.: Tidal stirring and phytoplankton bloom dynamics in an estuary, J. Mar. Res., 49, 203–221, https://doi.org/10.1357/002224091784968611, 1991.

485

De Boyer Montégut, C., Madec, G., Fischer, A. S., Lazar, A., and Iudicone, D.: Mixed layer depth over the global ocean: An examination of profile data and a profile-based climatology, J. Geophys. Res., 109, 2004JC002378, https://doi.org/10.1029/2004JC002378, 2004.

490   Díez-Minguito, M. and de Swart, H. E.: Relationships Between Chlorophyll-a and Suspended Sediment Concentration in a High-Nutrient Load Estuary: An Observational and Idealized Modeling Approach, J. Geophys. Res.: Oceans, 125, e2019JC015188, https://doi.org/10.1029/2019JC015188, 2020.

Doyon, P. and Ingram, R. G.: Seasonal upper-layer T–S structure in the Gulf of St. Lawrence during the ice-free months, Deep
495   Sea Res. II, 47, 385–413, https://doi.org/10.1016/S0967-0645(99)00112-5, 2000.

Dreujou, E., McKindsey, C. W., Grant, C., Tréau de Coeli, L., St-Louis, R., and Archambault, P.: Biodiversity and Habitat Assessment of Coastal Benthic Communities in a Sub-Arctic Industrial Harbor Area, Water, 12, 2424, https://doi.org/10.3390/w12092424, 2020.

500

Ferrario, F., Araújo, C. A. S., Bélanger, S., Bourgault, D., Carrière, J., Carrier-Belleau, C., Dreujou, E., Johnson, L. E., Juniper, S. K., Mabit, R., McKindsey, C. W., Ogston, L., Picard, M. M. M., Saint-Louis, R., Saulnier-Talbot, É., Shaw, J.-L., Templeman, N., Therriault, T. W., Tremblay, J.-E., and Archambault, P.: Holistic environmental monitoring in ports as an opportunity to advance sustainable development, marine science, and social inclusiveness, Elem. Sci. Anth., 10, 00061,
505   https://doi.org/10.1525/elementa.2021.00061, 2022.

Fiedler, P. C.: Comparison of objective descriptions of the thermocline, Limnol. Oceanogr. Methods, 8, 313–325, https://doi.org/10.4319/lom.2010.8.313, 2010.

510   Fisheries and Ocean Canada, Sept-Îles-02780, https://www.marees.gc.ca/fr/stations/02780 Last access: 15 December 2024.

Galbraith, P. S.: Winter water masses in the Gulf of St. Lawrence, J. Geophys. Res.: Oceans, 111, https://doi.org/10.1029/2005JC003159, 2006.

515   Galbraith, P. S., Sévigny, C., Bourgault, D., and Dumont, D.: Sea Ice Interannual Variability and Sensitivity to Fall Oceanic Conditions and Winter Air Temperature in the Gulf of St. Lawrence, Canada, J. Geophys. Res.: Oceans, 129, e2023JC020784, https://doi.org/10.1029/2023JC020784, 2024a.

Galbraith, P. S., Blais, M., Lizotte, M., Cyr, F., Bélanger, D., Casault, B., Clay, S., Layton, C., Starr, M., Chassé, J., Azetsu-Scott, K., Coyne, J., Devred, E., Gabriel, C.-E., Johnson, C. L., Maillet, G., Pepin, P., Plourde, S., Ringuette, M., and Shaw, J.-L.: Oceanographic conditions in the Atlantic zone in 2023, Can. Tech. Rep. Hydrogr. Ocean Sci., 379 pp., 2024b.

Government of Canada: Données Historiques, Station Sept-Îles, https://climate.meteo.gc.ca/historical_data/search_historic_data_f.html, last access: 24 April 2025.

Government of Québec, ministère du Développement durable, de l'Environnement et des Parcs, Direction du patrimoine écologique et des parcs: Réserve écologique de la Matamec, Conservation Plan, 14 pp., 2011.

IPCC: Sections, in: Climate Change 2023: Synthesis Report. Contribution of Working Groups I, II and III to the Sixth Assessment Report of the Intergovernmental Panel on Climate Change, edited by: Lee, H. and Romero, J., IPCC, Geneva, Switzerland, 35-115, https://doi.org/10.59327/IPCC/AR6-9789291691647, 2023.

Janecki, M., Dybowski, D., Rak, D., and Dzierzbicka-Glowacka, L.: A New Method for Thermocline and Halocline Depth Determination at Shallow Seas, J. Phys. Oce., 52, 2205–2218, https://doi.org/10.1175/JPO-D-22-0008.1, 2022.

Joshi, N., Montero-Serrano, J.-C., Lefebvre, C., and Saulnier-Talbot, É.: Tracking Pre- and Post-Industrialization Changes in the Bay of Sept-Îles, Canada, Using Foraminifera as Bioindicators, Journal of Coastal Research, 41, https://doi.org/10.2112/JCOASTRES-24A-00009, 2025.

Laliberté, J. and Larouche, P.: Chlorophyll-a concentration climatology, phenology, and trends in the optically complex waters of the St. Lawrence Estuary and Gulf, J. Mar. Syst., 238, 103830, https://doi.org/10.1016/j.jmarsys.2022.103830, 2023.

Lefebvre, C.: Évaluation du potentiel des pigments comme bioindicateurs de la diversité bactérienne et algale dans un milieu côtier anthropisé (Baie de Sept-Îles, Québec), M.S. thesis, Université Laval, Québec, 2023.

Leppäranta, M., and Myrberg, K.: Topography and Hydrography of the Baltic Sea, in: Physical Oceanography of the Baltic Sea, Springer Praxis Books, Berlin, Heidelberg, 41-88, 2009.

Lim, A. S., Park, N. Y., Choi, H. S., Kang, S. U., Ok, J. H., and Yoo, Y. D.: Influence of environmental parameters on marine plankton diversity in the southern coastal waters of Korea: Emphasis on thermal stratification, Mar. Environ. Res., 203, 106829, https://doi.org/10.1016/j.marenvres.2024.106829, 2025.

Liu, B., De Swart, H. E., and De Jonge, V. N.: Phytoplankton bloom dynamics in turbid, well-mixed estuaries: A model study, Estuarine, Coast. Shelf Sci., 211, 137–151, https://doi.org/10.1016/j.ecss.2018.01.010, 2018.

555 Long, Z., Perrie, W., Chassé, J., Brickman, D., Guo, L., Drozdowski, A., and Hu, H.: Impacts of Climate Change in the Gulf of St. Lawrence, Atmos.-Ocean, 54, 337–351, https://doi.org/10.1080/07055900.2015.1029869, 2016.

Maske, H., Ochoa, J., Almeda-Jauregui, C. O., Ruiz-de la Torre, M. C., Cruz-López, R., and Villegas-Mendoza, J. R.: Near-surface temperature gradient in a coastal upwelling regime, J. Geophys. Res.: Oceans, 119, 4972–4982, 560 https://doi.org/10.1002/2014JC010074, 2014.

May, C. L., Koseff, J. R., Lucas, L. V., Cloern, J. E., and Schoellhamer, D. H.: Effects of spatial and temporal variability of turbidity on phytoplankton blooms, Mar. Ecol. Prog. Ser., 254, 111-128, 2003.

565 Nielsen, J. M., Sigler, M. F., Eisner, L. B., Watson, J. T., Rogers, L. A., Bell, S. W., Pelland, N., Mordy, C. W., Cheng, W., Kivva, K., Osborne, S., and Stabeno, P.: Spring phytoplankton bloom phenology during recent climate warming on the Bering Sea shelf, Prog. Oceanogr., 220, 103176, https://doi.org/10.1016/j.pocean.2023.103176, 2024.

Paquette, L., Le Hénaff, A., and Carrière, J.: Courants Marins, in: Observatoire Environnemental de la Baie de Sept-Îles, edited 570 by: Carrière., J., INREST, Sept-Îles, QC, Canada, 571-588, 2018.

Pärn, O., Friedland, R., Rjazin, J., and Stips, A.: Regime shift in sea-ice characteristics and impact on the spring bloom in the Baltic Sea, Oceanol., 64, 312–326, https://doi.org/10.1016/j.oceano.2021.12.004, 2022.

575 Port of Sept-Îles: https://www.portsi.com/port/, last access: 02 January 2025.

R Core Team: R: A language and environment for statistical computing, R Foundation for Statistical Computing, Vienna, Austria, https://www.R-project.org/, 2022.

580 Roden, C.M., and Raine, R.: Phytoplankton Blooms and a Coastal Thermocline Boundary along the West Coast of Ireland, Estuar. Coast. Shelf Sci., 39, 511-526, 1994.
Roegner, G. C., Seaton, C., and Baptista, A. M.: Climatic and Tidal Forcing of Hydrography and Chlorophyll Concentrations in the Columbia River Estuary, Estuaries and Coasts, 34, 281–296, https://doi.org/10.1007/s12237-010-9340-z, 2011.

585   Shaw, J.-L., Bourgault, D., and Dumont, D.: Hydrodynamique de la Baie de Sept-Îles, M.S. thesis, Université du Québec à Rimouski, Rimouski, QC, Canada, 2019.

Shaw, J.-L., Bourgault, D., Dumont, D., and Lefaivre, D.: Hydrodynamics of the Bay of Sept-Îles, Atmos.-Ocean, 10, 1–17, https://doi.org/10.1080/07055900.2022.2141605, 2022.

590

Stramska, M. and Jakacki, J.: Variability of chlorophyll a concentration in surface waters of the open Baltic Sea, Oceanol., 66, 365–380, https://doi.org/10.1016/j.oceano.2024.02.003, 2024.

Wang, D., Kuang, C., Wang, G., Liu, J., Song, W., Xing, R., and Zou, Q.: Factors Influencing the Spatio-Temporal Distribution
595   of Chlorophyll-a in Jinmeng Bay, China, J. Mar. Sci. Eng., 12, 384, https://doi.org/10.3390/jmse12030384, 2024.

Wei, X. and Zhao, H.: Spatiotemporal distribution of chlorophyll-a concentration in the south China sea and its possible environmental regulation mechanisms, Mar. Environ. Res., 204, 106902, https://doi.org/10.1016/j.marenvres.2024.106902, 2025.

600

Winslow, L., Read, J., Woolway, R., Brentrup, J., Leach, T., Zwart, J., Albers, S., and Collinge, D: _rLakeAnalyzer: Lake Physics Tools_. R package version 1.11.4.1, https://CRAN.R-project.org/package=rLakeAnalyzer, 2019.

Wu, Y.-L., Zhou, C.-X., and Zhang, Y.-S.: Vertical Profiles of Chl-a and Primary Productivity in the Middle Continental Shelf
605   Area and Eddy Area of the East China Sea, Chin. J. Ocean. Limnol, 20, 74–80, https://doi.org/10.1007/BF02846614, 2002.

Yasunaka, S., Ono, T., Sasaoka, K., and Sato, K.: Global distribution and variability of subsurface chlorophyll a concentrations, Ocean Sci., 18, 255–268, https://doi.org/10.5194/os-18-255-2022, 2022.